Organic Semiconductor g-C_3N_4 Modified TiO_2 Nanotube Arrays for Enhanced Photoelectrochemical Performance in Wastewater Treatment

Lingjuan Liu,[a, b] Guan Zhang,[a] John T. S. Irvine,*[a] and Yucheng Wu*[b]

g-C_3N_4 sensitized TiO_2 nanotube arrays (g-C_3N_4/TNTs) were fabricated by using a simple solid sublimation and transition (SST) method using urea as precursor. The photoelectrochemical (PEC) performances were evaluated in this work. It is proposed that the g-C_3N_4 layer can play dual roles: surface sensitization and passivation of TNTs surface trap states to inhibit charge recombination. The g-C_3N_4/TNTs exhibited significantly improved PEC performance compared with TNTs under blue light (460 nm) irradiation. The g-C_3N_4/TNTs prepared from 3 g urea showed the highest photocurrent density of approximately 65 μA cm^{-2}, which is almost 10 times as high as that of TNTs. Furthermore, g-C_3N_4/TNTs showed enhanced photoelectrocatalytic degradation of methylene blue (MB) under the blue light irradiation. The stable performance of degradation of MB in multicycle tests suggests that the hybrid g-C_3N_4/TNT electrode could be used as a low-cost photoelectrode material for wastewater treatment processes.

Introduction

In recent years, semiconductor photo(electro)-catalysis has been widely studied in solar energy driven environmental remediation and energy conversion processes such as organic pollutants degradation[1–3] and H_2 generation.[4–6] TiO_2 is considered as one of the most widely used photocatalysts due to its superior optical and electronic properties, high chemical stability, low toxicity, and low cost. Among various nanostructures of TiO_2, highly ordered TiO_2 nanotube arrays (TNTs) fabricated through electrochemical anodization of titanium foils attract much interest because of the large specific surface area and precisely oriented nature of the nanotube arrays, which improve the charge-collection efficiency by promoting faster electron/hole transport and slower recombination.[7] Besides, TNTs on a titanium substrate can be easily recycled after using as a photocatalyst or photoelectrode, compared with free standing TNTs. However, the wide band gap of TiO_2 (3.0–3.2 eV) allows it to be activated only by the UV light, which accounts for only 4–5 % of solar energy. To broaden the photoresponse of TNTs into the visible light region and enhance the separation rate of photo-induced electrons and holes, a number of approaches have been attempted, such as the addition of non-metal atoms (N,[8] C,[9] B,[10,11] etc.), doping with metal ions (Fe,[12] Zr,[13] Cr[14]), decoration with noble metals (Ag,[15] Pt,[16] Au[17] etc.), and modification with inorganic semiconducting materials with narrower band-gaps such as CdS,[18] CdSe,[19] Cu_2O,[20] Fe_2O_3,[21] and $SrTiO_3$.[22] On the other hand, many surface defects normally exist on the TNT electrodes prepared by the electrochemical anodization and thermal annealing processes, which act as recombination centers for charge carriers. Surface passivation of nanostructured photoelectrodes by a thin layer of metal oxides is an effective method to inhibit charge recombination induced by surface defects. For example, a thin coating of an alumina layer onto hematite electrodes significantly improved the water oxidation performance in PEC water splitting.[23]

Recently, polymeric graphitic carbon nitride (g-C_3N_4) was reported as a novel metal-free organic photocatalyst by Wang et al.,[24] and it has attracted intense interest for its applications in photocatalytic hydrogen production and degradation of organic pollutants under visible light, considering its suitable band gap energy (≈2.7 eV) and high conduction band (CB) level (≈−1.3 eV at pH 7 vs NHE).[25,26] The g-C_3N_4 powder can be synthesized by thermal annealing of different precursors such as cyanamide, dicyandiamide, and melamine.[27] Besides, urea has also been used as a low-cost precursor to prepare g-C_3N_4.[28,29] Following the pioneering work by Wang et al., some efforts have been devoted into coupling g-C_3N_4 and TiO_2 photocatalysts for enhanced visible light activity. For example, Yan et al. fabricated a TiO_2–g-C_3N_4 composite by ball-milling of the mixture TiO_2 and C_3N_4

[a] Dr. L. Liu, Dr. G. Zhang, Prof. J. T. S. Irvine
School of Chemistry, University of St Andrews
St Andrews, Fife, KY16 9ST, Scotland (United Kingdom)
Fax: (+44) 1334 463808
E-mail: jtsi@st-andrews.ac.uk
Homepage: http://ch-www.st-andrews.ac.uk/staff/jtsi/group/

[b] Dr. L. Liu, Prof. Y. Wu
School of Materials Science and Engineering
Hefei University of Technology
Hefei 230009 (PR China)
Fax: (+86) 551 62904517
E-mail: ycwu@hfut.edu.cn

powder,[30] whereas Wang et al. prepared g-C_3N_4 modified TiO_2 nanorod arrays by chemical vapor deposition (CVD) using melamine as precursor.[31] To our best knowledge, there are no reports on the fabrication of organic g-C_3N_4 semiconductor-modified TNTs as a photoelectrode.

In this work, a novel and facile method for preparing g-C_3N_4 modified TNTs was developed using melamine sublimation-based solid sublimation and transition (SST). A tube-in-tube structure was formed by coating the TNT walls with thin layer amorphous g-C_3N_4 using the SST process with urea as precursor. The surface coating of g-C_3N_4 onto the TNTs plays dual roles: surface sensitization of TNTs and passivation of the TNT surface trap states, which enhances the PEC performance of the TNTs. Compared with the bare TNTs, the organic–inorganic hybrid g-C_3N_4 and TNT composite (g-C_3N_4/TNTs) shows much higher photocurrent density and decoloration towards methyl blue (MB) dye in aqueous solution under blue light (460 nm) irradiation powered by a 5 W light-emitting diode (LED) lamp. The low-power LED lamp illumination-assisted photoelectrochemical decoloration of MB dye on the g-C_3N_4/TNTs electrode may provide a promising tool for wastewater treatment, in combination with other advanced technologies (e.g., adsorption, biological degradation).

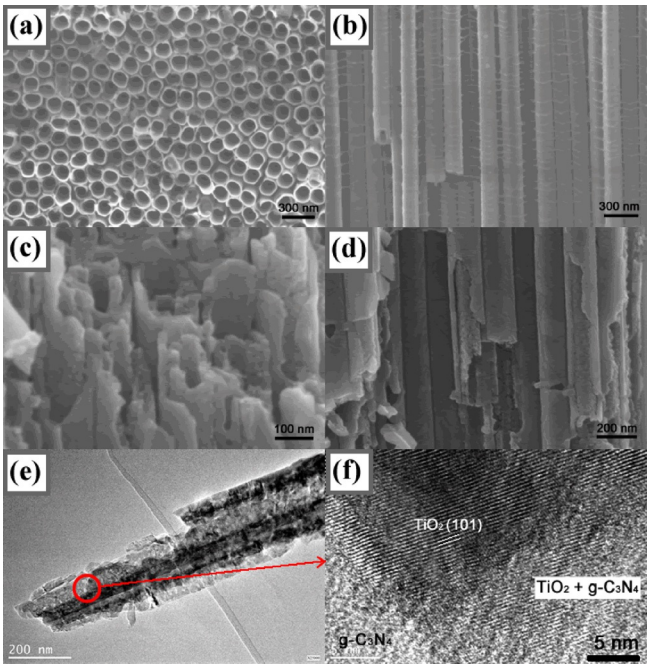

Figure 1. a, b) FESEM images of TNTs; c, d) FESEM images of g-C_3N_4/TNTs (3 g); e, f) HRTEM images of g-C_3N_4/TNTs (3 g).

Results and Discussion

Morphology and structure of materials

The organic g-C_3N_4 layer was deposited onto the inside walls of TNTs using urea powder as precursor as shown in Scheme 1. According to the literature,[32] urea decomposes to ammonia and isocyanic acid upon fast heating from 300 °C; furthermore, the isocyanic acid is able to convert to cyanamide, which can trimerize to melamine in the presence of in situ generated NH_3 gas. As the sublimation point of melamine is approximately 335 °C,[24] it is reasonable to expect that some portion of melamine would sublime into the gas phase in the partially sealed crucible and further diffuse into the TNTs during the thermal treatment. Upon further thermal treatment at approximately 400 °C, melamine is converted into polymeric melem. Prolonged heating at 550 °C produces a polycondensed g-C_3N_4 network. The sublimated melamine gas is adsorbed on the rough surfaces of the TNT walls and further condensed into a thin g-C_3N_4 coating layer. The SST deposition of g-C_3N_4 onto TNTs was confirmed by scanning electron microscopy (SEM) and high-resolution transmission electron microscopy (HRTEM). Figure 1 shows the morphologies of the as-prepared TNTs and g-C_3N_4/TNTs (3 g) examined by field emission SEM and HRTEM. From the images of the TNTs (Figure 1a, b), the highly ordered TNTs synthesized by the electrochemical anodization of the Ti foil show an average inner diameter of approximately 125 nm, wall thickness of 15 nm, and length of 5 μm. The representative SEM images of crushed g-C_3N_4/TNTs (3 g) are shown in Figure 1c, d. A thin layer of g-C_3N_4 was grafted onto the inner TNT walls at a thickness of approximately 23 nm, forming the tube-in-tube structure. The tube-in-tube structure of the corresponding g-C_3N_4/TNTs (3 g) sample was further identified by TEM and HRTEM as shown in Figure 1e, f. The light-gray parts confined inside of crystallized TiO_2 nanotube are assumed as g-C_3N_4 in accordance with the observation from SEM. From the HRTEM image in Figure 1f, the lattice spacing of the crystallized TNTs wall was observed to be approximately 0.352 nm, which corresponds to the (101) plane of anatase TiO_2 (JPCDS 21-1272). The amorphous phase shown in the left-bottom area is assigned to g-C_3N_4 according to reported results.[33] The overlapped crystalline and amorphous regions in the right-bottom area are assumed to be the amorphous g-C_3N_4 wrapped inside of TNTs.

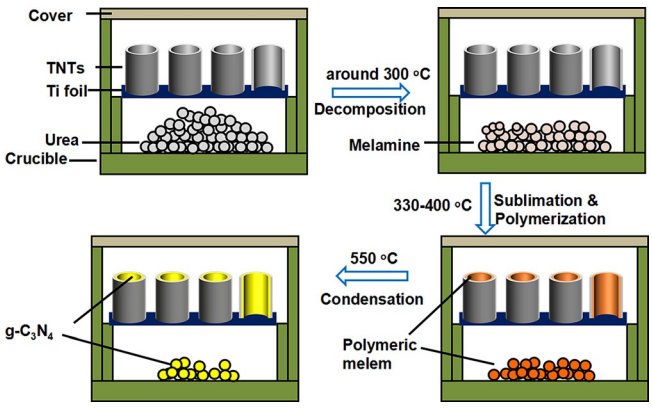

Scheme 1. Embedding g-C_3N_4 into TNTs by using SST with urea powder as precursor (cross-sectional view).

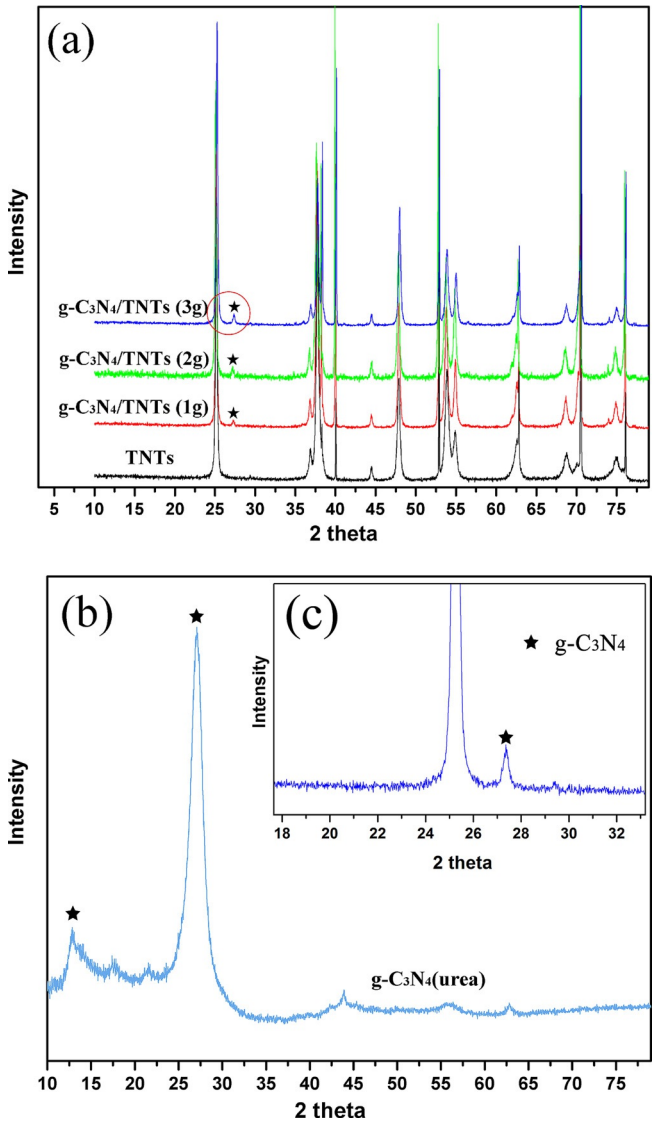

Figure 2. XRD spectra: a) TNTs and g-C_3N_4/TNTs (1 g, 2 g, 3 g); b) residual powder g-C_3N_4 after SST processing; c) magnified image of g-C_3N_4/TNTs (3 g).

Figure 2 shows the XRD patterns of bare TNTs, g-C_3N_4/TNTs (1 g, 2 g, 3 g), and residual g-C_3N_4 powder remaining on the crucible after SST processing. As observed in Figure 2a, the as-prepared bare TNTs and g-C_3N_4/TNTs show similar crystallized anatase patterns, which are in accordance with the HRTEM results. Compared to bare TNTs, g-C_3N_4/TNTs (1 g, 2 g, 3 g) all have tiny broad diffraction peaks at approximately 27.4°, which can be clearly observed from the enlarged image in Figure 2c. In comparison with the XRD patterns of g-C_3N_4 residual powder as shown in Figure 2b, this small peak at approximately 27.4° is assumed identified as g-C_3N_4 buried into nanotubes, as g-C_3N_4 (urea) shows the characteristic peaks of g-C_3N_4 at 13.1° and 27.4°, which are due to the stacking of conjugated aromatic system, as in graphite.[24] Upon increasing the amount of urea from 1 to 3 g, the peak intensity of g-C_3N_4 appears stronger, which indicates that a larger amount of g-C_3N_4 was formed. The X-ray diffraction (XRD) results indicate that g-C_3N_4 was successfully deposited into the TNT nanotubes by using urea as a precursor.

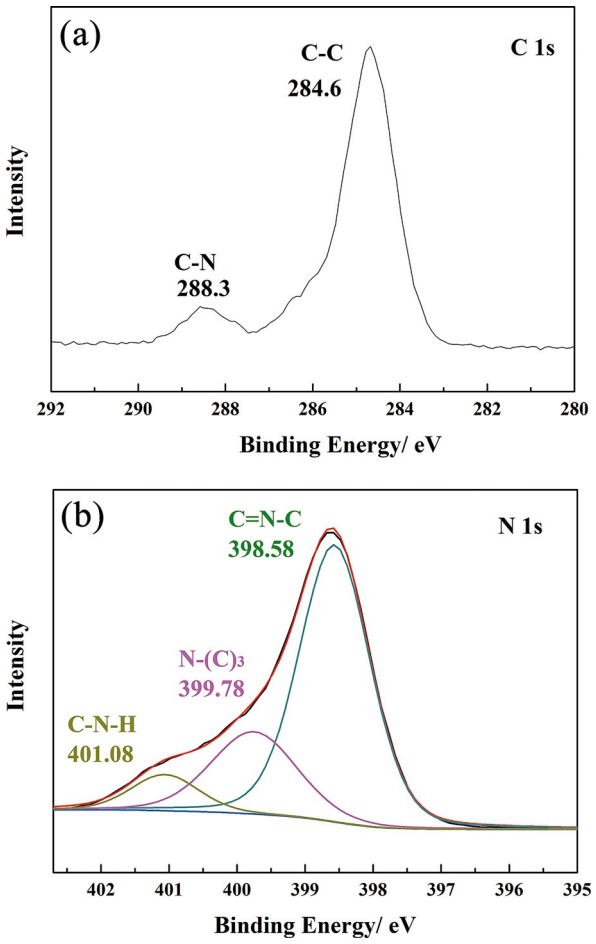

Figure 3. XPS spectrum of g-C_3N_4/TiO_2-TNTs (3 g): a) C1s; b) N1s.

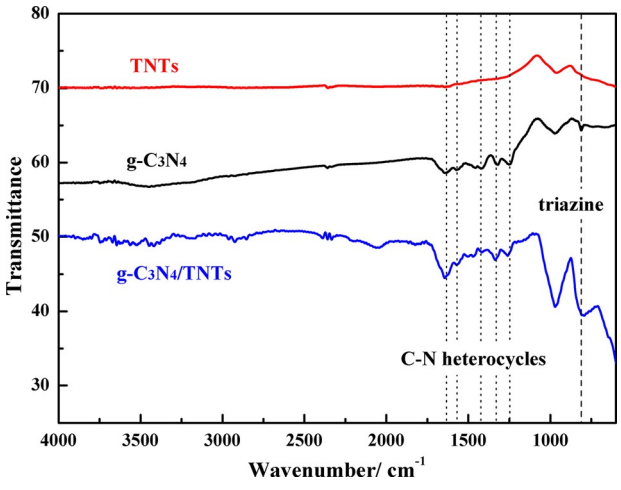

Figure 4. FTIR spectra of TNTs, g-C_3N_4 and g-C_3N_4/TNTs (3 g).

Chemical composition of materials

X-ray photoelectron spectroscopy (XPS) and FTIR analysis were used to confirm the amorphous g-C_3N_4 coating on the TNTs, as shown in Figure 3 and Figure 4. From the XPS spectrum of C1s shown in Figure 3a, two peaks can be distinguished centered at 284.6 and 288.3 eV, respectively. The peak at 284.6 eV is assigned to the adventitious hydrocarbon from the XPS instrument, and the other at 288.3 eV is identified a C–N–C coordination.[34] In the N1s spectrum (Figure 3b), the peaks at 398.58, 399.78, and 401.08 eV are assigned as sp^2 hybridized nitrogen (C=N–C), sp^3 tertiary nitrogen (H–N–$(C)_3$), and amino functional groups with a hydrogen atom (C–NH_x), respectively.[28]

Figure 4 illustrates the FTIR spectra of TNTs, g-C_3N_4, and g-C_3N_4/TNTs (3 g). Compared with TNTs, in the FTIR spectra of g-C_3N_4 and g-C_3N_4/TNTs (3 g), there are several strong bands in the 1200–1650 cm^{-1} region with peaks of at approximately 1263, 1335, 1415, 1570, and 1640 cm^{-1}, which correspond to the typical stretching mode of CN heterocycles. The band near 808 cm^{-1} is attributed to out-of-plane bending modes of C–N heterocycles. A broad band near 3140 cm^{-1} corresponds to the stretching modes of terminal NH_2 or NH groups at the defect sites of the aromatic ring. Based on the results from the XPS and FTIR spectra, it is concluded that the material coated onto the TNT walls is organic g-C_3N_4.

UV/Vis spectra

The UV/Vis spectra of the samples are shown in Figure 5. TNTs primarily absorb ultraviolet light below 390 nm, which is ascribed to the intrinsic band gap absorption of TiO_2 (≈3.2 eV). However, a broad absorption tail appeared in the range of 400–600 nm, which can be assigned to the surface defect sites created during the thermal annealing process as well as light scattering by the pores.[35,36] After g-C_3N_4 modification, the absorption tail in the visible region was slightly reduced for all of the g-C_3N_4/TNTs samples, probably because the thin layer of g-C_3N_4 coated onto the TNTs reduced the defect sites on the TNT surfaces. However, the clear shift of the absorption edge by incorporation of g-C_3N_4 into TNTs was not observed. One possible explanation is that the mass of g-C_3N_4 loaded into TNTs compared to the TNTs matrix is not sufficient enough to induce the clear band-gap change. On the other hand, the light scattering by the TNT walls may also account for this.

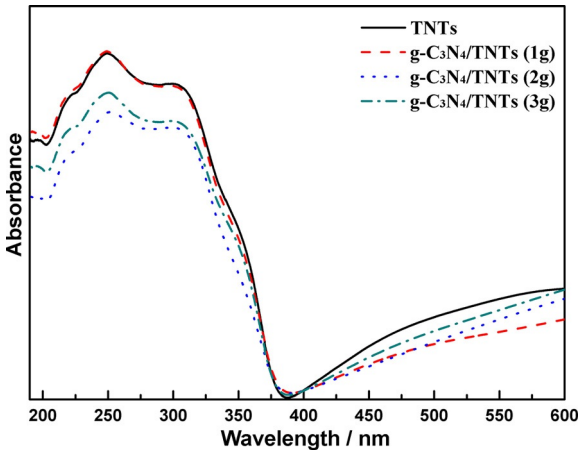

Figure 5. UV/Vis spectra of TNTs and g-C_3N_4/TNTs (1 g, 2 g, 3 g).

Photoelectrochemical studies

The photoelectrochemical performance was measured using a three-electrode system with the as prepared samples (TNTs and g-C_3N_4/TNTs) as working electrodes, a Ag/AgCl electrode as reference electrode, and a Pt mesh as counter electrode. A 5 W LED ModuLight with monochromatic light was used as visible light source with a 0.1 M Na_2SO_4 aqueous solution as the supporting electrolyte. The photocurrent of the TNTs and g-C_3N_4/TNTs with an active area of 1 cm^2 was measured at a scanning rate of 20 mV s^{-1} from −0.5 V to 1.0 V under blue light (460 nm). From Figure 6a the photocurrent of the TNT electrode was observed to be lower due to the poor visible light absorbance of TiO_2. The surface defects induced a small photocurrent under visible light irradia-

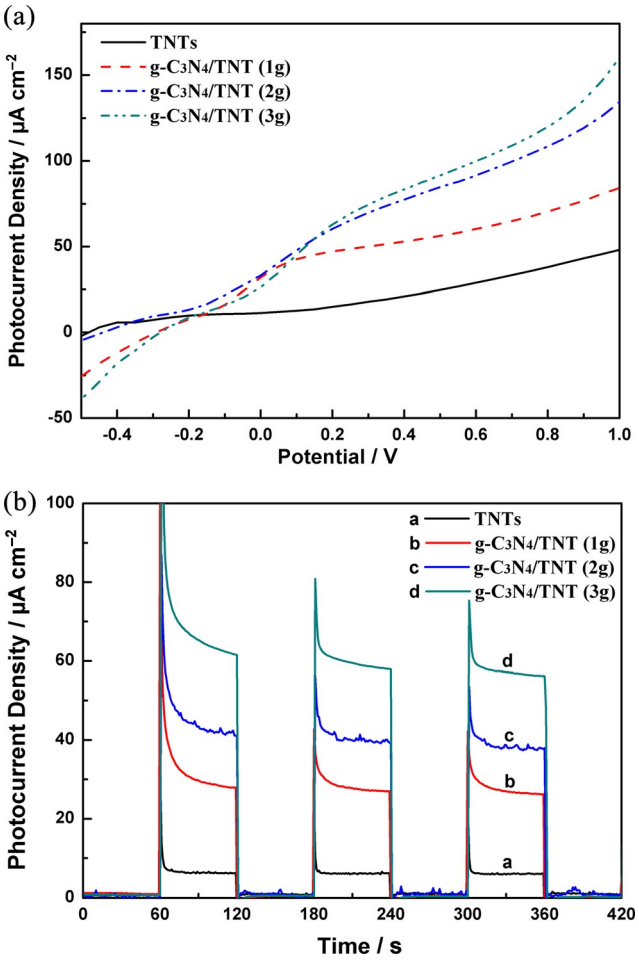

Figure 6. a) Photocurrents and b) transient photocurrents of TNTs and g-C_3N_4/TNTs (1 g, 2 g, 3 g).

tion. In comparison to the bare TNTs, the photocurrent responses of g-C_3N_4/TNTs are markedly enhanced. The enhancement in the photocurrent is ascribed to the dual roles of the g-C_3N_4 coating: surface sensitization and passivation of surface defects. It is known that the CB level of g-C_3N_4 is more negative than the CB level of TiO_2. Upon photo-excitation by the 460 nm illumination, the generated electrons transfer from the CB of g-C_3N_4 to the CB of TiO_2, which induces the visible light photoelectrochemical activity. On the other hand, some surface defect sites were created on the TNTs during the thermal treatment process as shown in the UV/Vis spectra. These defect sites would be removed as recombination centers for charge carriers by loading a thin layer of g-C_3N_4. As a result, the overall PEC performance of g-C_3N_4/TNTs under visible light is significantly enhanced. It is observed that increasing the amount of urea precursor (1 g to 3 g) leads to enhancement of the photocurrents. The highest photocurrent was obtained from the sample prepared using 3 g urea as precursor in which more g-C_3N_4 powder was deposited onto the TNTs walls by the SST process. However, further increasing the urea loading did not enhance the photocurrent significantly. The transient photocurrent response of the electrodes was also tested under blue light illumination with a light on/off circle of 60 s at a bias potential of 0.5 V vs. Ag/AgCl electrode. As shown in Figure 6b, a fast and steady photocurrent response was observed for each switch on and off on all of the electrodes, and the photocurrent response was totally reversible. The photocurrent density of the g-C_3N_4/TNTs (3 g) is almost 10 times as that of TNTs. The great enhancement can be ascribed to the improved charge separation and transportation efficiency through the interaction between the g-C_3N_4 and TNTs.

Figure 7 shows the time profiles of photoelectrochemical decolorization of MB with different TNTs and g-C_3N_4/TNTs samples. The photoelectrocatalytic degradation processes were performed at a bias potential of 0.5 V vs. Ag/AgCl electrode under blue light (460 nm). In Figure 7a, we observe that the decolorization rate for TNTs is approximately 18% after illumination for 10 h. After modification with g-C_3N_4, all of the g-C_3N_4/TNTs samples show much higher decolorization efficiencies, which are in accordance with the results of photocurrent response. The g-C_3N_4/TNTs (3 g) shows the highest decolorization rate (≈55%), which is improved by approximately 3.0 times against bare TNTs. For comparison, the electrochemical decolorization (3 g-electro) and photocatalytic decolorization (3 g-photo) of MB were performed under identical conditions without photo-illumination or applying a bias potential, respectively. Without light illumination, there was no decolorization at all. Under photo-illumination, the concentration of MB was only slightly decreased. As shown in Scheme 2, the mechanism of the photoelectrocatalytic decomposition of the MB dye can be described as follows: upon visible light illumination, the organic g-C_3N_4 was excited and electron–hole pairs were generated. As mentioned previously, the CB of g-C_3N_4 is more negative than the CB of TiO_2, and the photoinduced electrons directly transfer to the CB of TiO_2, which results in an effective separation of the photoinduced electrons and holes. Besides, the external electric field forced the electrons to move from working electrode to the counter electrode, the rest of the photogenerated holes reacted with H_2O to produce OH radicals, which are responsible for the oxidation of organic compounds. The enhanced photoelectrocatalytic performance of g-C_3N_4/TNTs is ascribed to the construction of a heterojunction of two semiconductors as well as the applied bias potential voltage, both of which facilitated the separation of photoinduced electron–hole pairs and charge transfer. To assess the stability of the electrodes, the g-C_3N_4/TNTs (3 g) were

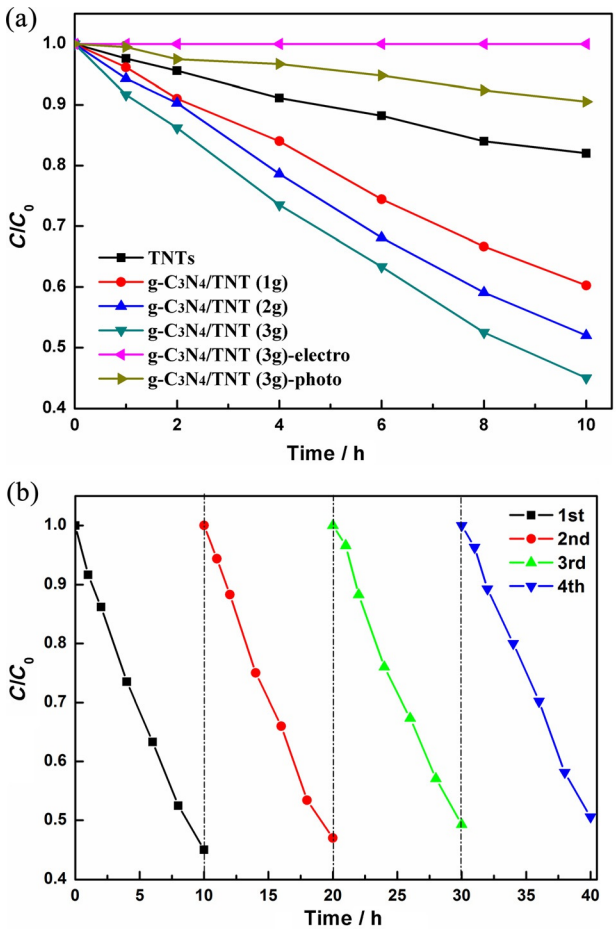

Figure 7. a) The photoelectrochemical decolorization of MB dye using TNTs and different g-C_3N_4/TNTs; b) multicycle tests of g-C_3N_4/TNTs (3 g) for the decolorization of MB.

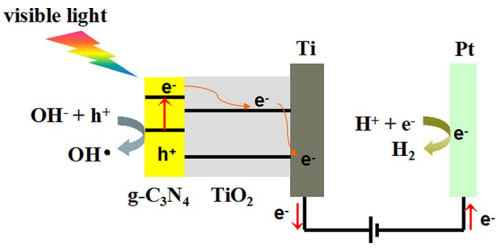

Scheme 2. Charge-transfer process at the g-C_3N_4/TNTs photoelectrode for photoelectrocatalytic degradation of MB.

tested four times for the photoelectrocatalytic decolorization of MB. As shown in Figure 7b, the decolorization rate of MB for each cycle varies only slightly, which indicates the good stability of g-C_3N_4/TNTs. The stable performance during the multicycle tests suggests that the hybrid g-C_3N_4/TNT electrode could be used as a low-cost photoelectrode material in the advanced wastewater treatment processes.

Conclusions

The organic semiconductor g-C_3N_4 was successfully deposited onto TiO_2 nanotubes (TNTs) using urea as precursor by simple and facile solid sublimation and transition (SST). The thin amorphous organic g-C_3N_4 layer plays dual roles: surface sensitization and passivation of TNTs surface trap states to inhibit the charge recombination, which enhances the photoelectrochemical (PEC) performance under visible light irradiation. All of the modified samples show higher photocurrent responses and degradation rates towards methylene blue (MB) under blue light (460 nm) as compared to bare TNTs. The g-C_3N_4/TNTs (3 g) exhibited the highest photocurrent response and its photocurrent density was approximately 65 $\mu A\,cm^{-2}$, which is up to 10 times that of pure TNTs. In accordance, g-C_3N_4/TNTs (3 g) showed the highest photoelectrocatalytic degradation rate and stability towards the decolorization of MB.

Experimental Section

Fabrication of TNTs

Highly ordered TNTs were fabricated by potentiostatic anodization. Titanium foils (0.1 mm thickness, 99.6% purity) were degreased by sonication in acetone, highly pure water, and ethanol for 15 min, 10 min, and 5 min successively, then dried in air. A two-electrode configuration including a titanium foil acting as the anode and a piece of highly pure graphite ($50\times30\times5\ mm^3$) as the cathode was used. The electrolyte consisted of 0.1 M NH_4F dissolved in ethylene glycol (EG) with water content of 10 vol%. The anodization was performed at a constant voltage of 60 V for 2 h. All experiments were performed at room temperature unless otherwise stated.

After anodization, to wipe off the debris on the surface of the TNTs, the samples were sonicated in EG for 60 s and then rinsed with highly pure water and dried in air. Then the samples were annealed in air at 550 °C for 2 h with a heating/cooling rate of $2\,^{\circ}C\,min^{-1}$.

Synthesis of g-C_3N_4/TNTs

Deposition of g-C_3N_4 into TNTs was obtained using a facile SST process with urea as precursor, as shown in Scheme 1. Different amounts of urea (1.0, 2.0, and 3.0 g) were added in a home-made aluminum crucible, and the TNTs were placed 1 cm above the urea powders. The crucible was covered by aluminum foil and then heated at 550 °C for 4 h at a ramping rate of $8\,^{\circ}C\,min^{-1}$ in a muffle furnace. During the SST process, only a small amount of g-C_3N_4 polymer was successfully deposited into the TNTs, whereas the majority of as-prepared g-C_3N_4 powders remained on the bottom of crucible. The g-C_3N_4/TNTs made from 1.0, 2.0, and 3.0 g urea were denoted as g-C_3N_4/TNTs (1 g), g-C_3N_4/TNTs (2 g), and g-C_3N_4/TNTs (3 g), respectively.

Characterization of TNTs and g-C_3N_4/TNTs

The morphology of TNTs and g-C_3N_4/TNTs was characterized by field-emission scanning electron microscopy (FESEM, FEI Sirion 200) and transmission electron microscopy (FETEM, JEM-2100F). X-ray diffraction (XRD) was used to characterize the structure of the samples. The chemical states of the samples were analyzed by X-ray photoelectron spectroscopy (XPS, ESCALAB250). The Fourier transform infrared spectra (FTIR) of the samples were recorded using an FTIR spectrometer (Nicolet 67). The UV/Vis spectra were recorded using a UV/Vis spectrometer (V-650).

Photoelectrochemical measurement

The photoelectrochemical performance was measured using a three-electrode system with the samples as working electrode, a Ag/AgCl electrode as reference electrode, and a Pt mesh as counter electrode. A 5 W LED ModuLight with monochromatic light was used as the visible light source. A 0.1 M Na_2SO_4 aqueous solution was chosen as the supporting electrolyte. The photocurrents of the TNTs and g-C_3N_4/TNTs with an active area of 1 cm^2 were measured at a scanning rate of $20\,mV\,s^{-1}$ from −0.5 V to 1.0 V under blue light (460 nm) and the instantaneous photocurrent response was measured at a bias potential of 0.5 V vs. Ag/AgCl electrode under blue light. The photoelectrocatalytic degradation of methyl blue (MB) was performed by inserting the electrode into a 70 mL MB solution (10 μM) with an illuminated area of 6 cm^2, also at a bias potential of 0.5 V vs. Ag/AgCl electrode under blue light. Before light irradiation, the working electrode was put into the target MB solution in the dark for 30 min to allow the system to reach adsorption equilibrium. Sample aliquots were withdrawn at intervals for quantitative analysis by using a UV/Vis spectrophotometer (Lambda 35).

Acknowledgements

This work was supported by China Scholarship Council (CSC), Royal Society of Edinburgh (RSE), and Engineering and Physical Sciences Research Council (EPSRC).

Keywords: electrochemistry · photocatalysis · methylene blue · titanium dioxide · wastewater treatment

[1] K. Vinodgopal, D. E. Wynkoop, P. V. Kamat, *Environ. Sci. Technol.* **1996**, *30*, 1660.
[2] R. Asahi, T. Morikawa, T. Ohwaki, K. Aoki, Y. Taga, *Science* **2001**, *293*, 269.
[3] Y. Zhao, X. Zhang, Z. Jin, J. He, L. Jiang, Z. Liu, S. Nishimoto, T. Murakami, A. Fujishima, D. Zhu, *Appl. Catal. B* **2008**, *83*, 24.
[4] X. Chen, S. Shen, L. Guo, S. Mao, *Chem. Rev.* **2010**, *110*, 6503.
[5] M. Wu, A. Sápi, A. Avila, M. Szabó, J. Hiltunen, M. Huuhtanen, G. Tóth, Á. Kukovecz, Z. Kónya, R. Keiski, W. Su, H. Jantunen, K. Kordás, *Nano Res.* **2011**, *4*, 360.
[6] J. Zhang, P. Du, J. Schneider, P. Jarosz, R. Eisenberg, *J. Am. Chem. Soc.* **2007**, *129*, 7726.
[7] P. Roy, S. Berger, P. Schmuki, *Angew. Chem. Int. Ed.* **2011**, *50*, 2904; *Angew. Chem.* **2011**, *123*, 2956.

[8] R. P. Vitiello, J. M. Macak, A. Ghicov, H. Tsuchiya, L. F. P. Dick, P. Schmuki, *Electrochem. Commun.* **2006**, *8*, 544.
[9] J. H. Park, S. Kim, A. J. Bard, *Nano Lett.* **2006**, *6*, 24.
[10] N. Lu, X. Quan, J. Li, S. Chen, H. Yu, G. Chen, *J. Phys. Chem. C* **2007**, *111*, 11836.
[11] J. Li, N. Lu, X. Quan, S. Chen, H. Zhao, *Ind. Eng. Chem. Res.* **2008**, *47*, 3804.
[12] L. Sun, J. Li, C. L. Wang, S. F. Li, H. B. Chen, C. J. Lin, *Solar Energy Mater. Solar Cells* **2009**, *93*, 1875.
[13] Y. Li, Y. Xiang, S. Peng, X. Wang, L. Zhou, *Electrochim. Acta* **2013**, *87*, 794.
[14] S. Zhang, Y. Chen, Y. Yu, H. Wu, S. Wang, B. Zhu, W. Huang, S. Wu, *J. Nanopart. Res.* **2008**, *10*, 871.
[15] X. He, Y. Cai, H. Zhang, C. Liang, *J. Mater. Chem.* **2011**, *21*, 475.
[16] N. T. Nguyen, J. E. Yoo, M. Altomare, P. Schmuki, *Chem. Commun.* **2014**, *50*, 9653.
[17] Z. Zhang, L. Zhang, M. N. Hedhili, H. Zhang, P. Wang, *Nano Lett.* **2013**, *13*, 14.
[18] W. Sun, Y. Yu, H. Pan, X. Gao, Q. Chen, L. Peng, *J. Am. Chem. Soc.* **2008**, *130*, 1124.
[19] J. A. Fernandes, P. Migowski, Z. Fabrim, A. F. Feil, G. Rosa, S. Khan, G. J. Machado, P. F. P. Fichtner, S. R. Teixeira, M. J. L. Santos, J. Dupont, *Phys. Chem. Chem. Phys.* **2014**, *16*, 9148.
[20] Y. Hou, X. Li, X. Zou, X. Quan, G. Chen, *Environ. Sci. Technol.* **2009**, *43*, 858.
[21] S. K. Mohapatra, S. Banerjee, M. Misra, *Nanotechnology* **2008**, *19*, 315601.
[22] J. Zhang, J. H. Bang, C. Tang, P. V. Kamat, *ACS Nano* **2010**, *4*, 387.
[23] F. Le Formal, N. Tetreault, M. Cornuz, T. Moehl, M. L. Gratzel, K. Sivula, *Chem. Sci.* **2011**, *2*, 737.
[24] X. Wang, K. Maeda, A. Thomas, K. Takanabe, G. Xin, J. M. Carlsson, K. Domen, M. Antonietti, *Nat. Mater.* **2009**, *8*, 76.
[25] F. Su, S. C. Mathew, G. Lipner, X. Fu, M. Antonietti, S. Blechert, X. Wang, *J. Am. Chem. Soc.* **2010**, *132*, 16299.
[26] Y. Zheng, J. Liu, J. Liang, M. Jaroniec, S. Qiao, *Energy Environ. Sci.* **2012**, *5*, 6717.
[27] Y. Wang, X. Wang, M. Antonietti, *Angew. Chem. Int. Ed.* **2012**, *51*, 68; *Angew. Chem.* **2012**, *124*, 70.
[28] Y. Zhang, J. Liu, G. Wu, W. Chen, *Nanoscale* **2012**, *4*, 5300.
[29] J. Liu, T. Zhang, Z. Wang, G. Dawson, W. Chen, *J. Mater. Chem.* **2011**, *21*, 14398.
[30] H, Yan, H. Yang, *J. Alloys Compd.* **2011**, *509*, L26.
[31] J. Wang, W. Zhang, *Electrochim. Acta* **2012**, *71*, 10.
[32] D. Mitoraj, H. Kisch, *Chem. Eur. J.* **2010**, *16*, 261.
[33] X. Xu, G. Liu, C. Randorn, J. T. S. Irvine, *Int. J. Hydrogen Energy* **2011**, *36*, 13501.
[34] S. C. Yan, Z. S. Li, Z. G. Zou, *Langmuir* **2010**, *26*, 3894.
[35] H. Zhu, B. Yang, J. Xu, Z. Fu, M. Wen, T. Guo, S. Fu, J. Zuo, S. Zhang, *Appl. Catal. B* **2009**, *90*, 463.
[36] J. G. Yu, H. G. Yu, B. Cheng, X. J. Zhao, J. C. Yu, W. K. Ho, *J. Phys. Chem. B* **2003**, *107*, 13871.

Received: April 15, 2015
Revised: June 10, 2015
Published online on July 17, 2015

